

Modeling ice-shelf cavities using Lagrangian elements

A.A. Stern,¹, A. Adcroft¹ and O. Sergienko¹, G. Marques¹, R. Hallberg¹

2 **Key Points:**

3

- 4 • A novel modeling framework is developed to model breakable ice shelves and ice-shelf cavities
5 using Lagrangian elements, held together by numerical bonds.
- 6 • The ocean circulation beneath a (static) Lagrangian ice shelf is almost indistinguishable
7 from the circulation beneath an Eulerian ice-shelf model run in an identical configuration.
- 8 • The similarity between the models provides a proof of concept for the Lagrangian model,
9 allowing the Lagrangian model to be used simulations involving tabular iceberg calving.

A. A. Stern, Geophysical Fluid Dynamics Laboratory, Princeton University

A. Adcroft, Geophysical Fluid Dynamics Laboratory, Princeton University

O. Sergienko, Geophysical Fluid Dynamics Laboratory, Princeton University

G. Marques, Geophysical Fluid Dynamics Laboratory, Princeton University

R. Hallberg, Geophysical Fluid Dynamics Laboratory, Princeton University

10 Abstract.

11 The current generation of ice-ocean models is unable to represent ice-shelf
12 calving in a physically realistic way despite its controlling role of the mass
13 balance and extent of Antarctic ice shelves. This is primarily due to static
14 Eulerian approach of the current ice-shelf/sub-ice-shelf cavity models that
15 does not allow separation and modification of computational domains that
16 would represent breaking of pieces of an ice shelf that would become freely
17 floating icebergs. In this study we develop a new ice-shelf cavity model where
18 the ice shelf is constructed out of Lagrangian elements that are bonded to-
19 gether by numerical bonds. This Lagrangian framework allows for large pieces
20 of the ice shelf to break away and become tabular icebergs. We test this La-
21 grangian ice -shelf model by simulating the circulation within a (static) ide-
22 alized ice-shelf cavity, which was developed as part of the Marine Ice Ocean
23 Modeling Inter-comparison Project (MISOMIP). The Lagrangian model re-
24 sults are compared to results of an Eularian model simulations with iden-
25 tical configuration. Results show that the Lagrangian and Eularian models
26 are almost indistinguishable. The similarly between the Eularian and Lagrangian
27 models in a static ice-shelf configuration provides a proof of concept for the
28 Lagrangian model, and means that we can confidently use Lagrangian ice-
29 shelf models to extend the capabilities of ice-shelf-cavity models.

1. Introduction

Satellite observations show that ice-shelf decay occurs via two main processes: melting and breaking [Depoorter et al , 2013; Rignot et al , 2013]. Each of these is responsible for approximately half of the ice-shelf decay, and each influences the surrounding ocean (and ice-shelf geometry) in a distinct way. Melting at the base of ice shelves causes fluxes of freshwater into the ice-shelf cavity. The input of buoyant meltwater creates rising density plumes, which are guided along the ice-shelf base, and help drive ocean circulation beneath the ice shelves [MacAyeal , 1984; Holland and Feltham , 2006]. Over time, melting at the ice-shelf base can erode the ice shelf, gradually altering the ice-shelf geometry. In contrast, iceberg calving causes sudden changes to the ice-shelf geometry, and releases giant icebergs into the ocean. After calving, these tabular icebergs can travel large distances and impact ocean hydrography [Martin and Adcroft , 2010; Stern et al , 2015], sea-ice formation [Robinson et al , 2012; Stern et al , 2016] and ocean biology [Smith et al , 2007; Vernet et al , 2012; Biddle et al , 2015] many miles away.

Modeling the ocean beneath the ice shelves presents a unique set of challenges, since (i) the presence of ice shelves provides a quasi-rigid upper boundary for the ocean model which is not encountered elsewhere in the ocean, and (ii) melting and breaking ice shelves imply changing ocean boundary conditions which present numerous numerical difficulties.

The earliest models of ocean ice-shelf cavities were developed using static ice shelves with a fixed shape [Hellmer and Olbers , 1989; Determan and Gerdes , 1994; Grosfeld et al , 1997; Holland and Jenkins , 2001; Losch , 2008]. In these models, ice-shelf melting was represented through salinity and temperature fluxes, while the ice-shelf geometry

51 remained unchanged. Later models of ice-shelf cavities allowed the ice-shelf geometry
52 to evolve as the ice shelf melted, permitting the study of coupled ocean-ice phenomena
53 [Gladish et al , 2012; Sergienko , 2013]. More recently, dynamic ice-shelf models have
54 been coupled to the ocean cavity, allowing the study of grounding line migration which is
55 of key importance for sea level rise projections [Grosfeld and Sandhger , 2004; Goldberg
56 et al , 2012; De Rydt and Gudmundsson , 2016; Seroussi et al , 2017].

57 All models of ice-shelf cavities to date have omitted ice-shelf breaking and iceberg
58 detachment. This is because (i) there is much uncertainty about the physics that govern
59 ice-shelf breaking [Benn et all , 2007; Alley et al , 2008; Levermann et al , 2012; Bassis
60 and Jacobs , 2013], and (ii) current models of ice-shelf cavities represent the ice shelves on
61 static Eularian grids, which do not lend themselves to modeling iceberg detachment and
62 drift. In contrast, existing *iceberg* models represent icebergs as Lagrangian particles, since
63 this is a convenient way to model discrete objects traveling over large distances [Bigg et
64 al , 1997; Gladstone et al , 2001; Martin and Adcroft , 2010; Marsh et al , 2015]. To date
65 there has been no real effort to synthesize these two approaches (i.e.: to combine ice shelf
66 and iceberg models).

67 In this study we develop a new ice-shelf cavity model where the ice shelf is simulated
68 with Lagrangian elements [Stern et al , 2017]. In this model, the ice shelf is constructed
69 out of Lagrangian elements which are bonded together by numerical bonds (see schematic
70 Figures 1). This Lagrangian framework allows for large pieces of the ice shelf to break away
71 and become tabular icebergs. An example of this enhanced capability of the Lagrangian
72 model is demonstrated in Figures 2, which shows a tabular iceberg drifting away from an
73 idealized ice shelf (see Stern et al [2017] for more details).

74 However, before analyzing the improved capabilities of the Lagrangian ice-shelf model,
75 it is necessary to thoroughly test and benchmark the Lagrangian ice-shelf model in a
76 more familiar configuration. To do this we compare the Lagrangian ice-shelf-cavity model
77 to existing Eularian model in a static ice-shelf configuration. For this comparison, we
78 use the model configuration developed as part of the Marine Ice Ocean Modeling Inter-
79 comparison Project (MISOMIP). The goals of this study are (i) to introduce and describe
80 the Lagrangian ice-shelf model, and (ii) to prove that the Lagrangian model can replicate
81 the behavior of an Eularian ice-shelf model when modeling ocean cavities beneath static
82 ice shelves. Demonstrating that the Lagrangian model compares well to more traditional
83 Eularian models is a prerequisite for using the Lagrangian model to move beyond the ca-
84 pabilities of the Eularian model, and increases our confidence in more complex Lagrangian
85 simulations involving calving icebergs.

2. Lagrangian model description

86 The Kinematic Iceberg Dynamics (KID) model is a Lagrangian model that has been
87 developed in order to simulate ice-shelf cavities with breakable ice shelves. The model
88 represents ice shelves using Lagrangian elements joined together by numerical bonds. By
89 breaking these bonds, the model is able to simulate ice-shelf calving and iceberg breakup.

90 Although the ice elements do not move in the static ice-shelf experiment presented in
91 this paper, this configuration is a relevant test for the Lagrangian model, as it tests the
92 interpolation and aggregation between Eularian and Lagrangian grids, and also tests the
93 coupling between the ocean and ice-shelf models.

94 In this section we describe the fully dynamic Lagrangian ice-shelf model. We then
95 focus on element packing and interpolation between the Eularian and Lagrangian grids,

which are the parts of the model which are relevant to static ice simulations. A complete description of the KID model, including details of the momentum budget and element interactions can be found in Stern et al [2017].

2.1. Kinematic Iceberg Dynamics model

The KID model is a Lagrangian particle-based model, in that the objects of the model are Lagrangian elements. Each Lagrangian element represents a column of ice that is floating in the ocean. The elements have their own position, velocity, mass, and a set of dimensions, which can evolve in time. Each element moves according to its own momentum balance which is computed in the (Lagrangian) reference frame of the element. The elements experience oceanic, sea ice and atmospheric drag forces, as well as a forces due to sea surface height gradients, and the Coriolis force [Bigg et al , 1997; Gladstone et al , 2001; Martin and Adcroft , 2010; Stern et al , 2017]. The elements also interact with other elements and can be ‘bonded’ together by numerical bonds, which allow many elements to move together as a unit. By bonding many ice elements together, the model is able to form larger structures, such as tabular icebergs or ice shelves (Figures 1).

The thickness and extent of the Lagrangian elements change due to melting when they are exposed to above-freezing ocean mixed-layer temperatures. The melt rates of the elements are prescribed using parametrizations developed for iceberg and ice-shelf decay [Bigg et al , 1997; Holland and Jenkins, 1999; Gladstone et al , 2001; Martin and Adcroft , 2010]. The corresponding heat, salt and mass fluxes are passed to the ocean to simulate freshwater injection to the ocean surface.

2.2. Initializing element geometry and packing

116 The elements in the Lagrangian model are shaped as equally-sized regular hexagons.
117 We initialize the Lagrangian model by positioning the elements in a staggered lattice
118 of equally-size hexagons, so that the elements fit together and perfectly tile the ice-shelf
119 surface (Figures 1b). Hexagonal elements are used so that when adjacent pairs of elements
120 are bonded together, the network of bonds form equilateral triangles, which gives rigidity
121 to the larger structure [Stern et al , 2017]. **??? Maybe add some comments about accuracy**
122 **of continuity of fields like pressure etc on the discrete elements???**

2.3. Interpolation and aggregation onto the Lagrangian grid

123 When constructing ice shelves using the Lagrangian model, the collection of elements
124 can be thought of as being a ‘Lagrangian grid’ for the ice shelf. In this framework the
125 nodes of the Lagrangian grid (elements) can move at every time step, altering the shape
126 of the ice shelf. This is in contrast to the more traditional approach of modeling ice
127 shelves on an Eulerian grid, where the grid is fixed in time. Using a Lagrangian grid is
128 a convenient framework for modeling breakable ice shelves since it allows pieces of the
129 ice-shelf grid to break away from the ice shelf and become part of the iceberg grid [Stern
130 et al , 2017].

131 In the experiments presented in this study, the ice-shelf model is coupled to an ocean
132 model, which is runs on a static Eulerian grid. At every time step, ice-shelf fields are
133 passed from the ice-shelf model to the ocean model and from the ocean model to the
134 ice-shelf model. Four ocean (mixed layer) fields are passed from the ocean model to the
135 ice-shelf model: temperature, salinity and zonal and meridional velocities. These fields
136 are interpolated onto the Lagrangian elements using a bilinear interpolation scheme.

137 At the end of a ice-shelf model time step, ice-shelf fields are aggregated from the elements
138 back onto the Eularian ocean grid, and are then passed from the ice-shelf model to the
139 ocean model. The aggregation from the Lagrangian grid to the Eularian ocean grid is
140 done in a way which is consistent with the shape of the elements. For the purposes of
141 aggregation, we assume that the elements have surface areas that are shaped as regular
142 hexagons. Element's properties are aggregated from the Lagrangian grid to the Eularian
143 grid by exactly calculating the fraction of an element that is intersects each ocean grid
144 cell, and dividing the element's properties between the ocean grid cell in proportion to
145 that fraction. ??? This part is a bit hard to follow, it needs more explanation. Don't
146 know whether a schematic could help. ???

2.4. Lagrangian vs Eularian ice-shelf model

147 In the next section, simulations using the Lagrangian ice-shelf model are compared to
148 simulations using an Eularian ice-shelf model with an an identical configuration. While
149 the internal framework and grids of the Eularian and Lagrangian ice-shelf models are
150 quite different, both models are coupled to the ocean model using the same coupling
151 structure. Five fields are passed from the ice-shelf models to ocean model: mass, surface
152 area, temperature flux, salinity flux and mass flux. The Eularian model uses the same
153 grid as the ocean model, while in the Lagrangian model these fields are aggregated onto
154 the ocean model grid before being passed through the coupler. Once in the ocean model,
155 these fields and are used to: (i) apply a pressure to the ocean surface, ??? This condition
156 is specific to MOM6. Some explanations are required either about MOM6 specifics or
157 how this could be handled in general. What if an ocean would be z-coordinate, what
158 would be an equivalent of this condition???(ii) alter the upper-ocean boundary condition

¹⁵⁹ to reflect that the ocean is covered by ice, another ambiguous statement and (iii) apply
¹⁶⁰ salt, temperature and mass fluxes associated with ice-shelf melting and freezing.

¹⁶¹ Since the coupling with the ocean model is handled in the same way for both the
¹⁶² Eulerian and Lagrangian models and both models are coupled to the same ocean model,
¹⁶³ any differences between the two models in the static ice-shelf configuration (using the
¹⁶⁴ same melt rate parametrization) are likely due to the interpolation/aggregation between
¹⁶⁵ the ice and ocean grids. By accurately aggregating fields from the Lagrangian grid to
¹⁶⁶ Eulerian ocean grids, we aim to make the Lagrangian ice-shelf model behave like the
¹⁶⁷ Eulerian ice-shelf model in static ice-shelf simulations.

3. Experiment Setup

3.1. Domain configuration

¹⁶⁸ In order for our simulations to be easily comparable to previous models of ice-shelf
¹⁶⁹ cavities, we use an experimental setup based on the configuration created for the Marine
¹⁷⁰ Ice Ocean Modeling Inter-comparison Project (MISOMIP) [Asay-Davis et al , 2016]. The
¹⁷¹ configuration consists of an idealized ice shelf in a rectangular domain $L_x = 80\text{km}$ long
¹⁷² and $L_y = 480\text{km}$ wide. The ice shelf is grounded on the southern side of the domain with
¹⁷³ the ice-shelf front at $y=650\text{km}$. The ice thickness and bottom topography of this setup
¹⁷⁴ are shown in Figure 3. The configuration is the same as that of the Ocean0 setup in the
¹⁷⁵ MISOMIP, with three changes made:

- ¹⁷⁶ 1. The ‘calving criteria’ used in the MISOMIP study (which states that all points in
¹⁷⁷ the ice shelf with thickness less than 100m are set to zero thickness) has not been used.
- ¹⁷⁸ 2. The ice shelf has been thickened on the flanks of the domain, so that the latitude of
¹⁷⁹ the grounding line increases away from the center of the ice shelf.

₁₈₀ 3. The ice shelf is configured to be symmetric about its meridional center line ($x = \frac{L_x}{2}$).

₁₈₁ This was achieved by using the average of the left and right flanks of the ice-shelf thickness.

₁₈₂ These three changes were made in order to make the circulation beneath the ice shelf

₁₈₃ easier to interpret.

3.2. Ocean Model

₁₈₄ The Lagrangian and Eulerian ice shelves are coupled to the MOM6 ocean model [Hall-

₁₈₅ berg et al , 2013]. The ocean model is run using a hybrid vertical coordinate system

₁₈₆ which blends a sigma-level and a z-level coordinate [Stern et al , 2017], implemented us-

₁₈₇ ing the ALE method [White et al , 2009]. In this vertical coordinate, model layers bend

₁₈₈ underneath surface topography (i.e.: the ice shelf), as they would in a sigma coordinate

₁₈₉ model, and intersect the bottom topography, as they would in a z-coordinate model. The

₁₉₀ model has 72 vertical layers and has a horizontal resolution of $\Delta x = 2$ km. The numerical

₁₉₁ simulations were all repeated using an isopycnal coordinate (without ALE regrinding-

₁₉₂ remapping). The results were qualitatively similar to the hybrid-coordinate results, and

₁₉₃ are therefore not presented here.

₁₉₄ The ocean parameters used in the simulations are as specified in the MISOMIP config-

₁₉₅ uration [Asay-Davis et al , 2016], and are shown in Table 1. The simulation is initialized

₁₉₆ from rest, with horizontally uniform initial ocean temperature and salinity profiles which

₁₉₇ vary linearly between specified open-ocean surface and bottom values: $T_{top} = -1.9^{\circ}\text{C}$,

₁₉₈ $T_{bottom} = 1.0^{\circ}\text{C}$, $S_{top} = 33.8$ psu, $S_{bottom} = 34.7$. The maximum ocean depth is

₁₉₉ $H_{ocean} = 720$ m. A sponge layer is used on the northern boundary, which relaxes back

₂₀₀ to the initial temperature and salinity with a relaxation time scale of $T_{sponge} = 0.1$ days

over a distance of 10 km. Melting is set to zero for ocean cells where the ocean column thickness is less than 10m.

3.3. Lagrangian ice-shelf simulations:

The Lagrangian ice shelf is created using 10882 Lagrangian hexagonal elements with sides of length $S = 0.98$ km . The positions of the hexagonal elements are initialized by packing them together in a space-filling staggered lattice. Gaps along the boundaries are filled in using smaller elements so that the total ice-shelf area is preserved. The initial mass of the ice elements is determined by a preprocessing inversion step, which is the inverse of the aggregation procedure discussed in Section 2.3.

3.4. Eulerian ice-shelf simulations:

The Eulerian ice-shelf simulation is performed using an existing Eulerian ice-shelf cavity model [Goldberg et al , 2012], which is an optional module of the the MOM6 ocean model. The ice shelf is initialized on the same grid as the ocean model with a horizontal resolution of $\Delta x = 2$ km. The ice-shelf thickness field is initialized using the same ice-shelf draft used for the Lagrangian model (Figure 3).

3.5. Sub-ice-shelf melting

The melt rates in both the Lagrangian and Eulerian ice-shelf simulations are calculated using the 3 equation model for ice-shelf decay [Holland and Jenkins, 1999]. In both experiments the ice shelf is held stationary. In the Eulerian code, this is achieved by setting the ice-shelf velocity to zero, while in Lagrangian ice shelf, the element velocities are set to zero. In both simulations, the ice shelf is thermodynamically active and is able to ‘melt’ but has a time-invariant thickness (as specified in the Ocean0 experiment

in the MISOMIP [Asay-Davis et al , 2016]). In this setup, ice-shelf melting generates temperature and salinity fluxes into the ocean, but does not change the thickness of the ice shelf / ice elements. This can be thought to represent an ice shelf in dynamic equilibrium where the melt is exactly balanced ice-shelf advection.

4. Results

4.1. Results from the Lagrangian ice-shelf simulation

The results from the Lagrangian ice-shelf simulation fit within the current understanding of ice-shelf cavity circulations based on ice-shelf observations [MacAyeal , 1984; Lewis and Perkin , 1986; Jacobs et al , 2011] and previous modeling efforts [Determan and Gerdes , 1994; Holland and Feltham , 2006; Losch , 2008]. The ocean temperatures inside the domain are warmer than the in-situ freezing point (Figure 4a), and cause melting at the ice-shelf base (Figure 5c). The meltwater entering the domain is more buoyant than the water around it, and rises along the ice shelf as a cool fresh plume (Figure 4). This injection of positive buoyancy at depth drives a clockwise circulation outside of the ice-shelf cavity (Figure 6a), providing the ice-shelf cavity with a continuous supply of warm water, which provides the thermal energy required for continuous ice-shelf melt.

The highest melt rates are observed within 100km of the grounding line (Figure 5a). These elevated melt rates are caused by the presence of warm water (Figure 5d) and increased ocean velocities (Figure 5c) near the grounding line, as well as the fact that freezing point of ice decreases with increasing pressure. Elevated melt rates are also seen near the ice front, caused by strong currents running along the ice-shelf front (Figure 5c).

4.2. Comparison of Lagrangian and Eulerian ice-shelf models

The Lagrangian ice-shelf model results are qualitatively similar to most of the simulations from the MISOMIP experiment [Asay-Davis et al , 2016], which use a similar configuration (see Section 3.4). To get a quantitative comparison, we compare the Lagrangian ice-shelf model results to a simulation using an Eulerian ice-shelf model with an identical configuration. The results show that two simulations are almost indistinguishable. This is demonstrated, for example, in Figures 6, which shows the time-averaged barotropic stream function of the Lagrangian (Figures 6a) and Eulerian (Figures 6b) simulations, and the difference between the two (Figures 6c). The difference between the Lagrangian and Eulerian barotropic stream functions are two orders of magnitude smaller than typical differences observed between simulations using different models in the MISOMIP [Asay-Davis et al , 2016]. The similarity of the Lagrangian and Eulerian simulations are also reflected in the fact that the simulations have very similar ice-shelf melt rates and ocean temperature/salinity profiles (shown in Figures S1 and Figures S2 in the supplementary materials).

The agreement between the Eulerian and Lagrangian simulations is a confirmation that the Lagrangian model is able to simulate sub-ice-shelf cavities as well as the Eulerian model does. This is a good starting point for moving beyond the capabilities of the Eulerian model.

??? This section is a bit thin. Perhaps it'd be worth looking at more fields and also discuss to under which circumstances differences between the KID and Eulerian models can be larger and start affecting simulations and the results ???

5. Conclusion

260 This study presents a new Lagrangian framework for modeling sub-ice-shelf cavities.
261 In this framework, the ice shelf is constructed out of many Lagrangian elements, which
262 are bonded together by numerical bonds. The collection of Lagrangian elements store the
263 ice-shelf properties. Unlike Eulerian grids, the nodes (elements) can move at every time
264 step, altering the shape of the ice shelf. This allows us to use the Lagrangian ice-shelf
265 model to large pieces of the ice-shelf breaking away from the ice shelf to becoming tabular
266 icebergs that are fully embedded in the ocean (Figures 2). This capability is currently
267 not possible using more traditional Eulerian models [Stern et al , 2017].

268 The framework capabilities are demonstrated by modeling the circulation beneath a
269 (static) idealized ice shelf, which was developed as part of the MISOMIP inter-comparison
270 project. The results from the Lagrangian ice-shelf model fit within our paradigm of
271 understanding for circulation within ice-shelf cavities: buoyant meltwater that enters the
272 ice-shelf cavity drives freshwater plumes at the ice-shelf base, which drives the circulation
273 within the cavity. The circulation, melt rates and ocean hydrography achieved using the
274 Lagrangian ice shelf compare well with other simulations in the MISOMIP experiments.

275 A direct comparison ecomparison between the Lagrangian and a Eulerian ice-shelf model
276 coupled to the same ocean model shows that the results are extremely similar. Differences
277 between the Lagrangian and Eulerian ice shelves models (resulting from interpolation
278 errors) are much smaller than the differences observed when changing the ocean vertical
279 coordinate system (for example). Demonstrating that the Lagrangian ice-shelf model is
280 able to reproduce the results of an Eulerian ice-shelf model in the same static ice-shelf

²⁸¹ configuration is a prerequisite developing more advanced Lagrangian ice-shelf models and
²⁸² represents a good benchmark test for new Lagrangian ice-shelf models.

References

- 283 Asay-Davis, X. S., S. L. Cornford, B. K. Galton-Fenzi, R. M. Gladstone, G. H. Gudmundsson, D. M. Holland, P. R. Holland, and D. F. Martin (2016), Experimental design for
284 three interrelated marine ice sheet and ocean model intercomparison projects: MIS-
285 MIP v. 3 (MISMIP+), ISOMIP v. 2 (ISOMIP+) and MISOMIP v. 1 (MISOMIP1).
286 *Geoscientific Model Development* 9, no. 7: 2471.
- 287 Arrigo, K. R., G. L. van Dijken, D. G. Ainley, M. A. Fahnestock, and T. Markus (2002).
288 Ecological impact of a large Antarctic iceberg. *Geophys. Res. Lett.*, 29(7).
- 289 Alley, R. B., H. J. Horgan, I. Joughin, K. M. Cuffey, T. K. Dupont, B. R. Parizek, S.
290 Anandakrishnan, and J. Bassis (2008), A simple law for ice-shelf calving. *Science* 322,
291 no. 5906, 1344-1344.
- 292 Bassis, J. N., and S. Jacobs (2013), Diverse calving patterns linked to glacier geometry.
293 *Nature Geoscience*, 6(10), 833-836.
- 294 Benn, D. I., C. R. Warren, and R. H. Mottram (2007). Calving processes and the dynamics
295 of calving glaciers. *Earth-Science Reviews*, 82(3), 143-179.
- 296 Bigg, G. R., Wadley, M. R., Stevens, D. P., and Johnson, J. A. (1997), Modeling the
297 dynamics and thermodynamics of icebergs. *Cold Regions Science and Technology*, 26(2),
298 113-135.
- 299 Borstad, C. P., A. Khazendar, E. Larour, M. Morlighem, E. Rignot, M. P. Schodlok, and
300 H. Seroussi (2012), A damage mechanics assessment of the Larsen B ice shelf prior to
301 collapse: Toward a physically-based calving law, *Geophys. Res. Lett.*, 39, L18502
- 302 Biddle, L. C., J. Kaiser, K. J. Heywood, A. F. Thompson and A. Jenkins (2015), Ocean
303 glider observations of iceberg-enhanced biological productivity in the northwestern Wed-
- 304

- 305 dell Sea, *Geophys. Res. Lett.*, 42, 459465.
- 306 De Rydt, J., and G. H. Gudmundsson (2016), Coupled ice shelf ocean modeling and
307 complex grounding line retreat from a seabed ridge. *J. of Geophys. Res.: Earth Surface*,
308 121(5), 865-880.
- 309 Dunne, J.P., J.G. John,, A.J. Adcroft, S.M. Griffies, R.W. Hallberg, E. Shevliakova,
310 R.J. Stouffer, W. Cooke, K.A. Dunne, M.J Harrison, and J.P. Krasting (2012), GFDL's
311 ESM2 global coupled climate-carbon Earth System Models. Part I: Physical formulation
312 and baseline simulation characteristics. *J. of Climate*, 25(19), 6646-6665.
- 313 Depoorter, M. A., J. L. Bamber, J. A. Griggs, J. T. M. Lenaerts, Stefan RM Ligtenberg,
314 M. R. van den Broek, and G. Moholdt (2013), Calving fluxes and basal melt rates of
315 Antarctic ice shelves. *Nature*, 502(7469), 89-92.
- 316 Determan J., Gerdes R. (1994), Melting and freezing beneath ice shelves: implications
317 from a three-dimensional ocean-circulation model. *Ann. Glaciol.*, 20, 413-419.
- 318 Dowdeswell, J. A., and J. L. Bamber (2007), Keel depths of modern Antarctic icebergs
319 and implications for sea-floor scouring in the geological record. *Marine Geology*, 243(1),
320 120-131.
- 321 Duprat, L. P., G. R. Bigg, and D. J. Wilton (2016), Enhanced Southern Ocean marine
322 productivity due to fertilization by giant icebergs. *Nature Geoscience*.
- 323 Eckert, E. R. G. (1950). Introduction to the Transfer of Heat and Mass. McGraw-Hill.
- 324 Gladstone, R. M., G. R. Bigg, and K. W. Nicholls. (2001), Iceberg trajectory modeling
325 and meltwater injection in the Southern Ocean (19782012). *J. of Geophys. Res.: Oceans*,
326 106(C9), 19903-19915.

- 327 Goldberg, D. N., C. M. Little, O. V. Sergienko, A. Gnanadesikan, R. Hallberg, and M.
328 Oppenheimer (2012), Investigation of land ice?ocean interaction with a fully coupled
329 ice-ocean model: 1. Model description and behavior. *J. of Geophys. Res.: Earth Surface*,
330 117(F2).
- 331 Gladish, C. V., D. M. Holland, P. R. Holland, and S. F. Price (2012), Ice-shelf basal
332 channels in a coupled ice/ocean model. *J. of Glaciol.*, 58(212), 1227-1244.
- 333 Grosfeld K., R. Gerdes, J. Determan (1997), Thermohaline circulation and interaction
334 between ice shelf cavities and the adjacent open ocean. *J. Phys. Oceanogr.*, **102**, C7,
335 15959-15610.
- 336 Grosfeld, K., and H. Sandhger, (2004). The evolution of a coupled ice shelfocean system
337 under different climate states. *Global and Planetary Change*, 42(1), 107-132.
- 338 Hallberg, R., A. Adcroft, J. P. Dunne, J. P., Krasting, R. J., and Stouffer (2013), Sensitiv-
339 ity of twenty-first-century global-mean steric sea level rise to ocean model formulation.
340 *J. of Climate*, 26(9), 2947-2956.
- 341 Holland D. M., Jenkins A. (2001), Adaptation of an isopycnic coordinate ocean model for
342 the study of circulation beneath ice shelves. *Mon. Wea. Rev.*, 129, 1905-1927.
- 343 Holland P. R. and D. L. Feltham (2006), The effects of rotation and ice shelf topography
344 on frazil-laden Ice Shelf Water plumes. *J. Phys. Oceanogr.*, 36, 2312-2327.
- 345 Holland, D. M., and A. Jenkins (1999), Modeling thermodynamic ice-ocean interactions
346 at the base of an ice shelf. *J. of Phys. Oceanogr.* 29.8, 1787-1800.
- 347 Hellmer H.H., Olbers D. J. (1989), A two-dimensional model for the thermohaline circu-
348 lation under an ice shelf. *Antarctic Science*, 1, 325- 336.

- ³⁴⁹ Hopkins, M. A. (1996). On the mesoscale interaction of lead ice and floes. *J. of Geophys. Res.: Oceans*, 101(C8), 18315-18326.
- ³⁵¹ Jakobsen, T. (2001). Advanced character physics. In *Game Developers Conference*, Vol. 3.
- ³⁵³ Jenkins, A., P. Dutrieux, S. S. Jacobs, S. D. McPhail, J. R. Perrett, A. T. Webb, and D. White (2010), Observations beneath Pine Island Glacier in West Antarctica and implications for its retreat. *it Nature Geo.*, 3(7), 468-472.
- ³⁵⁶ Jacobs, S. S., A. Jenkins, C. F. Giulivi, and P. Dutrieux (2011). Stronger ocean circulation and increased melting under Pine Island Glacier ice shelf. *Nature Geo.*, 4(8), 519-523.
- ³⁵⁸ Jongma, J. I., E. Driesschaert, T. Fichefet, H. Goosse, and H. Renssen (2009), The effect of dynamic-thermodynamic icebergs on the Southern Ocean climate in a three-dimensional model, *Ocean Modell.*, 26, 104113.
- ³⁶¹ Lewis E.L. and R.G. Perkin (1986), Ice pumps and their rates. *J. of Geophys. Res.*, 91, 11756-11762.
- ³⁶³ Losch, M. (2008). Modeling ice shelf cavities in az coordinate ocean general circulation model. *J. of Geophys. Res.: Oceans*, 113(C8).
- ³⁶⁵ Li, B., H. Li, Y. Liu, A. Wang and S. Ji (2014), A modified discrete element model for sea ice dynamics. *Acta Oceanologica Sinica*, 33(1), 56-63.
- ³⁶⁷ Liu, M. B. and G. R. Liu (2010), Smoothed particle hydrodynamics (SPH): an overview and recent developments. *Archives of computational methods in engineering*, 17(1), 25-76.
- ³⁷⁰ Lichy, C., and H. H. Hellmer (2001). Modeling giant-iceberg drift under the influence of sea ice in the Weddell Sea, Antarctica. *J. of Glaciol.*, 47(158), 452-460.

- 372 Levermann, A., T. Albrecht, R. Winkelmann, M. A. Martin, M. Haseloff, and I. Joughin.
373 (2012), Kinematic first-order calving law implies potential for abrupt ice-shelf retreat.
374 *The Cryosphere*, 6(2), 273-286.
- 375 Martin, T., and Adcroft, A. (2010), Parameterizing the fresh-water flux from land ice
376 to ocean with interactive icebergs in a coupled climate model. *Ocean Modelling*, 34(3),
377 111-124.
- 378 Marsh, R., V. O. Ivchenko, N. Skliris, S. Alderson, G. R. Bigg, G. Madec, A. T. Blaker
379 Y. Aksenov, B. Sinha, A.C. Coward, and J.L. Sommer (2015), NEMOICB (v1. 0):
380 interactive icebergs in the NEMO ocean model globally configured at eddy-permitting
381 resolution. *Geoscientific Model Development* 8, no. 5 (2015): 1547-1562.
- 382 MacAyeal D.R. (1984), Thermohaline Circulation Below the Ross Ice Shelf: A Conse-
383 quence of Tidally Induced Vertical Mixing and Basal Melting. *J. Geophys. Res.*, 89,
384 597-606
- 385 Nicholls K.W. (1996), Temperature variability beneath Ronne Ice Shelf, Antarctica, from
386 thermistor cables. *J. Phys. Oceanogr.*, 11, 1199-1210.
- 387 Nicholls KW, Østerhus S, Makinson K (2009), Ice-Ocean processes over the continental
388 shelf of the southern Weddell Sea, Antarctica: a review. *Rev. Geophys.* 47(3).
- 389 Omelyan, I. P., M. I. Mryglod, and R. Folk (2002), Optimized Verlet-like algorithms for
390 molecular dynamics simulations. *Physical Review E*, 65(5), 056706.
- 391 Rignot, E., S. Jacobs, J. Mouginot, and B. Scheuchl (2013), Ice-shelf melting around
392 Antarctica. *Science*, 341, no. 6143 (2013): 266-270.
- 393 Robinson, N. J., M. J. M. Williams, P. J. Barrett, and A. R. Pyne (2010), Observations of
394 flow and ice-ocean interaction beneath the McMurdo Ice Shelf, Antarctica, *J. Geophys.*

- 395 *Res.*, 115, C03025
- 396 Pan, W., A. M. Tartakovsky, and J. J. Monaghan (2013). Smoothed particle hydrody-
397 namics non-Newtonian model for ice-sheet and ice-shelf dynamics. *J. of Comp. Phys.*,
398 242, 828-842.
- 399 Pralong, A., and M. Funk (2005), Dynamic damage model of crevasse opening and appli-
400 cation to glacier calving, *J. Geophys. Res.*, 110, B01309.
- 401 Seroussi H., Y. Nakayama, E.Y. Larour, D. Menemenlis, M. Morlighem, E. Rignot, and A.
402 Khazendar (2017), Continued retreat of Thwaites Glacier, West Antarctica, controlled
403 by bed topography and ocean circulation, *Geophys. Res. Lett.*, 44
- 404 Sergienko, O. V. (2013). Basal channels on ice shelves. *J. of Geophys. Res.: Earth Surface*,
405 118(3), 1342-1355.
- 406 Silva, T. A. M., Bigg, G. R., and Nicholls, K. W. (2006), Contribution of giant icebergs
407 to the Southern Ocean freshwater flux. *J. of Geophys. Res.: Oceans*, 111(C3).
- 408 Smith, K., B. Robison, J. Helly, R. Kaufmann, H. Ruhl, H., T. Shaw, and M. Vernet
409 (2007), Free-drifting icebergs: Hotspots of chemical and biological enrichment in the
410 Weddell Sea, *Science*, 317, 478482.
- 411 Stern, A. A., D. M. Holland, P. R. Holland, A. Jenkins and J. Sommeria (2014), The effect
412 of geometry on ice shelf ocean cavity ventilation: a laboratory experiment. *Experiments
413 in Fluids*, 55(5), 1-19.
- 414 Stern, A.A., Johnson, E., Holland, D.M., Wagner, T.J., Wadhams, P., Bates, R., Abra-
415 hamsen, E.P., Nicholls, K.W., Crawford, A., Gagnon, J. and Tremblay, J.E. (2015),
416 Wind-driven upwelling around grounded tabular icebergs. *J. of Geophys. Res.: Oceans*,
417 120(8), 5820-5835.

- 418 Stern, A. A., A. Adcroft, and O. Sergienko (2016), The effects of Antarctic iceberg calv-
419 ing?size distribution in a global climate model. *J. of Geophys. Res.: Oceans*, 121(8),
420 5773-5788.
- 421 Stern, A. A., A. Adcroft, O. Sergienko, G. Marques, R. Hallberg (2017), Modeling tabular
422 icebergs coupled to an ocean model. *Ocean Modeling*
- 423 Swope, W. C., H. C. Andersen, P. H. Berens, and K. R. Wilson (1982), A computer
424 simulation method for the calculation of equilibrium constants for the formation of
425 physical clusters of molecules: Application to small water clusters. *The Journal of
426 Chemical Physics* 76, no. 1, 637-649.
- 427 Tournadre, J., N. Bouhier, F. Girard-Ardhuin, and F. Rmy (2016), Antarctic icebergs
428 distributions 1992-2014. *J. Geophys Res: Oceans*.
- 429 Vernet, M., et al. (2012), Islands of ice: Influence of free-drifting Antarctic icebergs on
430 pelagic marine ecosystems, *Oceanography*, 25(3), 3839
- 431 Weeks, W. F., and W. J. Campbell (1973). Icebergs as a fresh-water source: an appraisal.
432 *J. of Glaciol.*, 12(65), 207-233.
- 433 White, L., A. Adcroft, and R. Hallberg (2009), High-order regriddingremapping schemes
434 for continuous isopycnal and generalized coordinates in ocean models. *J. of Comp.
435 Phys.*, 228(23), 8665-8692.

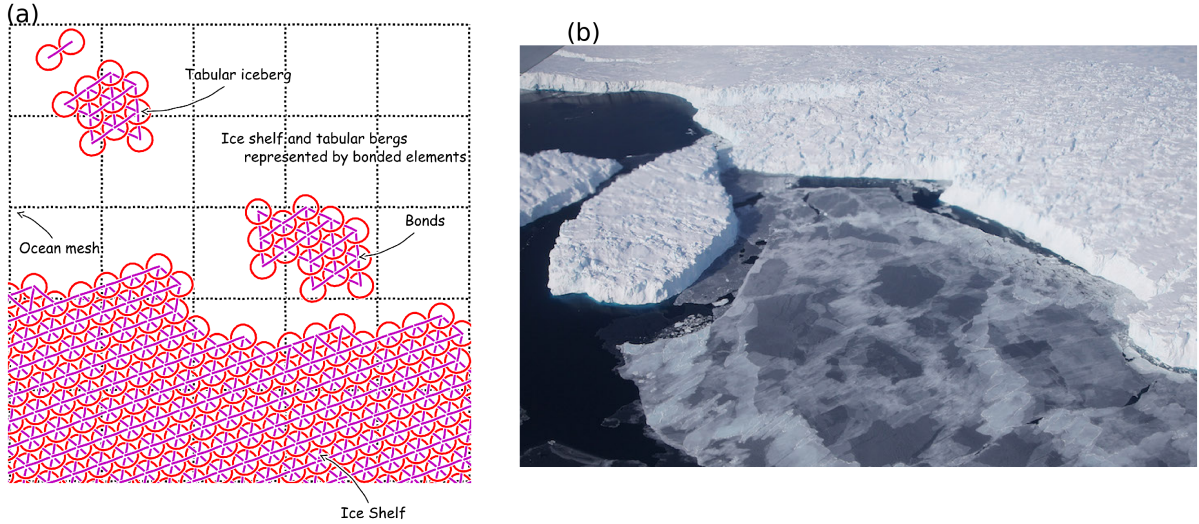


Figure 1. Schematic showing how ice shelves and tabular icebergs are constructed using Lagrangian elements. (a) Schematic of multiple ice elements that are joined together by numerical bonds (magenta lines) to form larger structures such as ice shelves and tabular icebergs. These numerical elements have finite extent and are able to interact with the ocean across multiple grid cells, and can interact with other elements. (b) Areal photograph of an ice shelf and tabular iceberg with elements superimposed over it to illustrate how the Lagrangian elements can be used to model ice shelves and tabular icebergs. In this schematic the ice elements (purple dots) are initialized in a staggered lattice covering the surface area of the iceberg. For purposes of mass aggregation, the ice elements are assumed to have hexagonal shape (red hexagons). For purposes of element interactions, the ice elements are assumed to be circular (black circles). Elements are initially bonded to adjacent elements using numerical bonds (magenta lines). These numerical bonds form equilateral triangles which give the shape rigidity. An ocean grid has been included (dashed cyan lines).

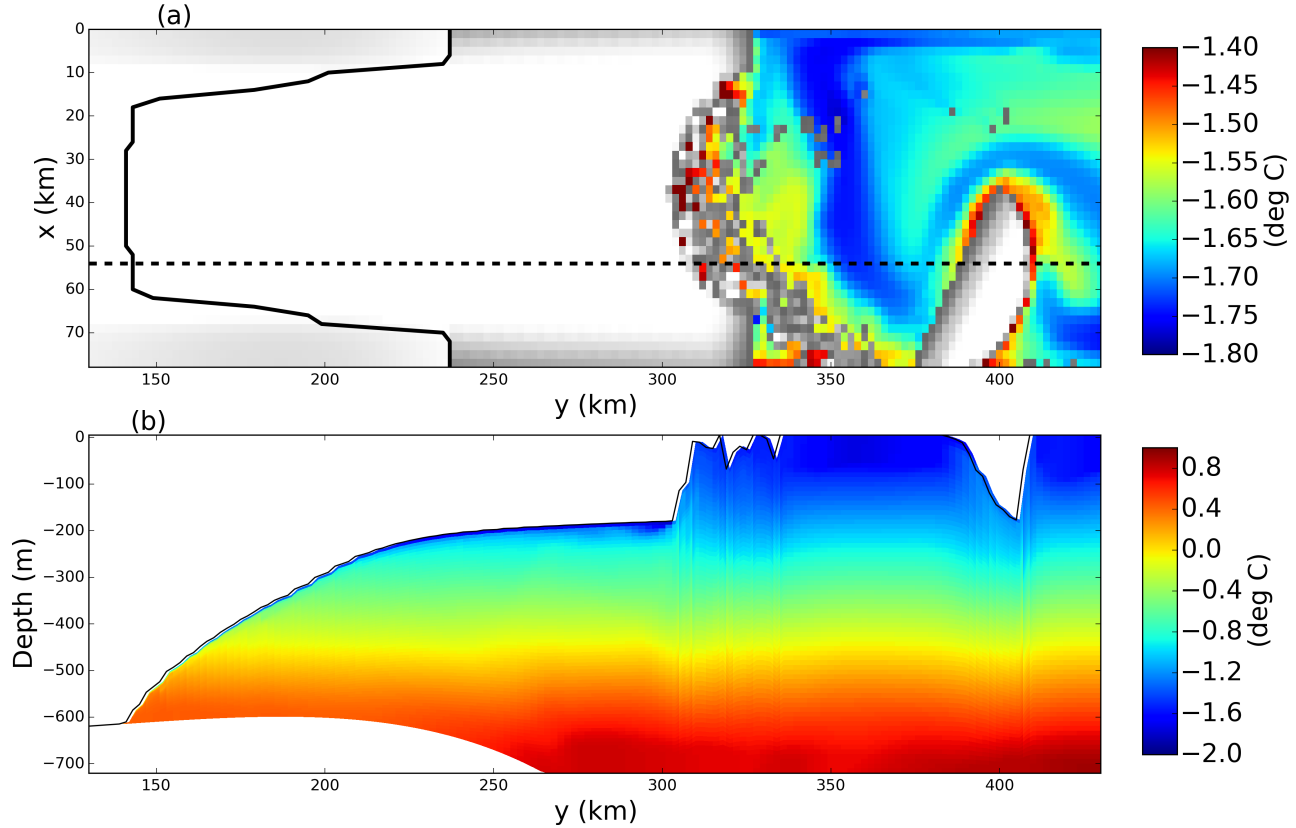


Figure 2. Snapshots of a simulation where a Lagrangian ice-shelf calves a tabular iceberg viewed (a) from above and (b) from the side. The snapshots are taken 30 days after calving. Panel (a) shows the sea surface temperature. Grid cells with ice mass $> 10^4$ kg are plotted in white, with grey shading indicating thinner ice. Panel (b) shows a vertical section of ocean temperature at $x=54$ km. The position of the vertical section is shown by the dashed line in panel (a). The solid line in panel (a) shows the position of the grounding line.

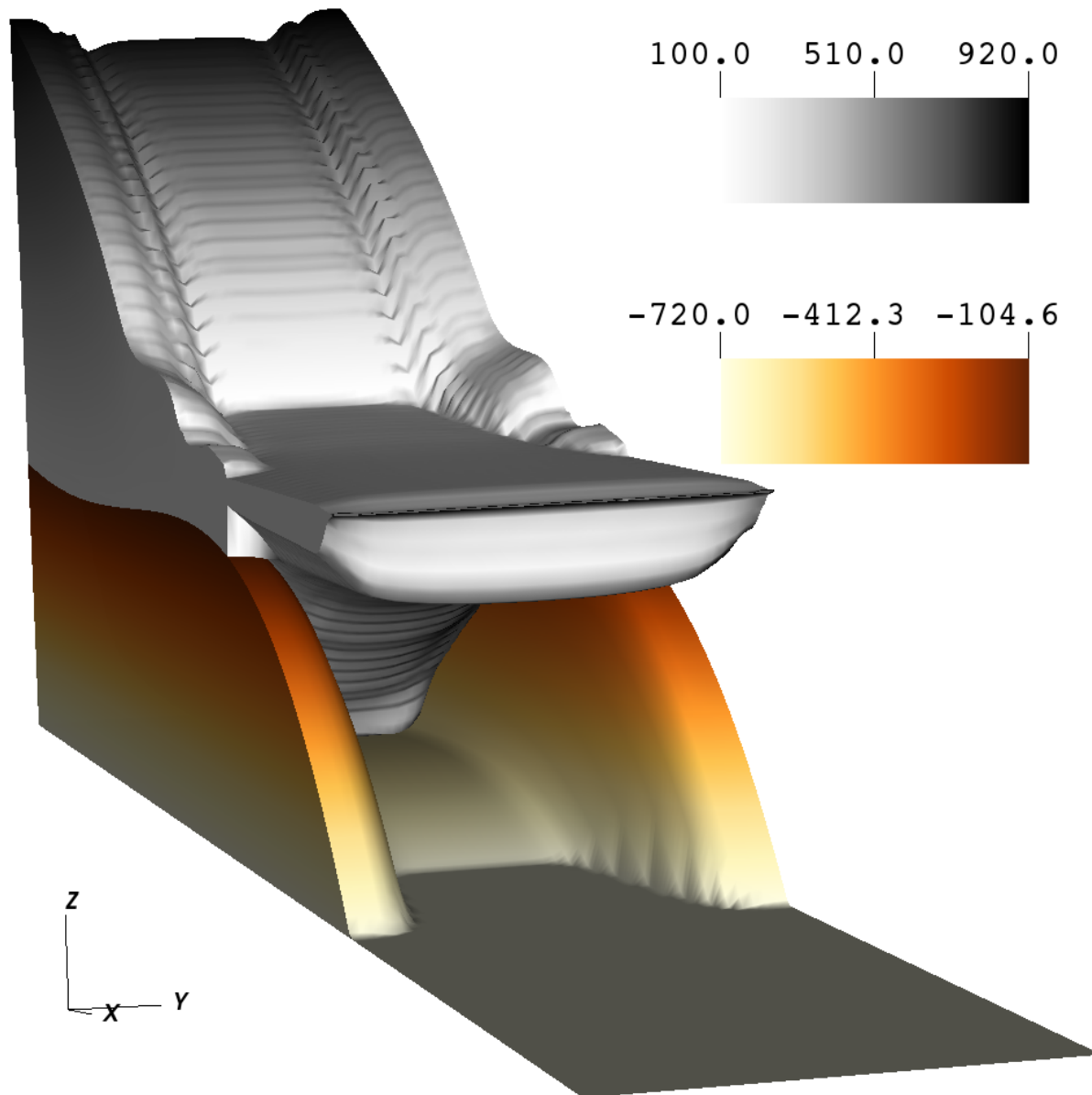


Figure 3. Ocean bottom topography and ice-shelf draft used in the Lagrangian and Eulerian static ice-shelf simulations

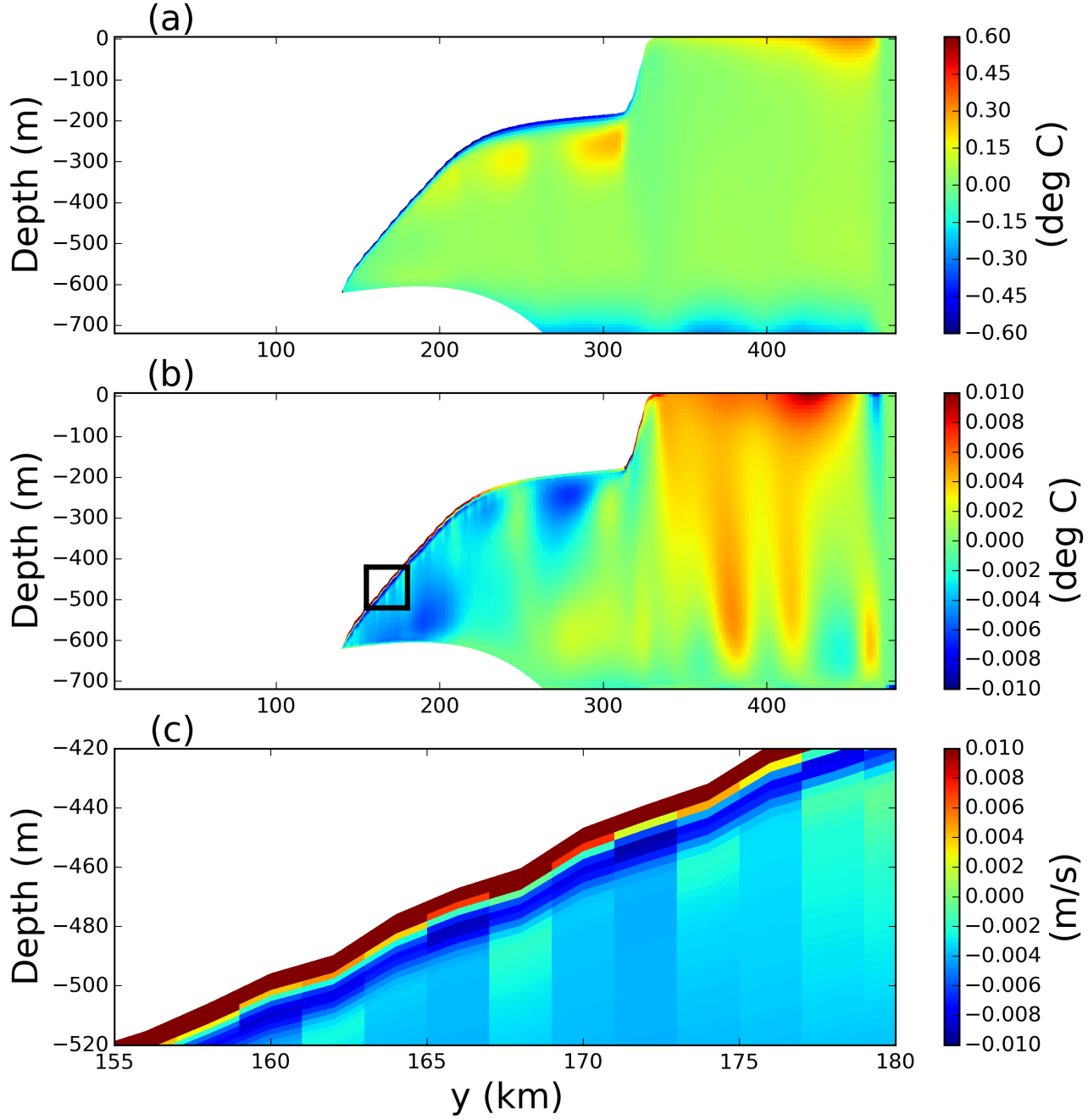


Figure 4. Snapshots of the static ice-shelf experiment taken after 5 years of model simulation, using the Lagrangian ice-shelf model coupled to the MOM6 ocean model. Panels show cross sections of the (a) ocean temperature anomaly relative to the initial temperature, and (b) the meridional ocean velocity. Panel (c) again shows the meridional ocean velocity, and is zoomed into the region near the ice-shelf base (the zoomed-in region is indicated with a black box (b)).

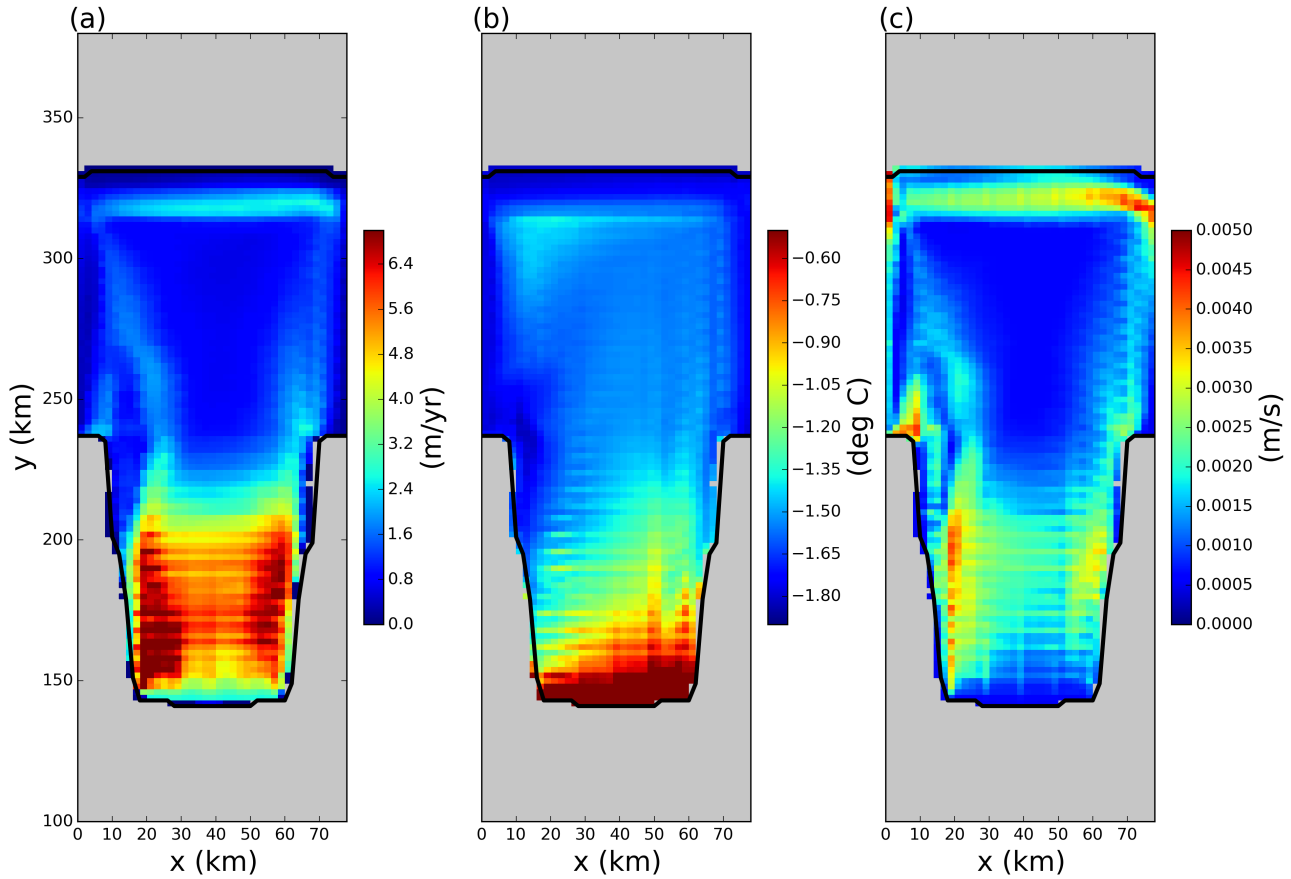


Figure 5. Results of the static ice-shelf experiment using the Lagrangian ice-shelf model coupled to MOM6. The three panels show 5 year time average of the (a) melt rate, (b) top-of-ocean temperature and (c) frictional velocity, u^* , at the base of the ice shelf. Fields are only shown in regions where the ice area fraction is ≥ 0.8 .

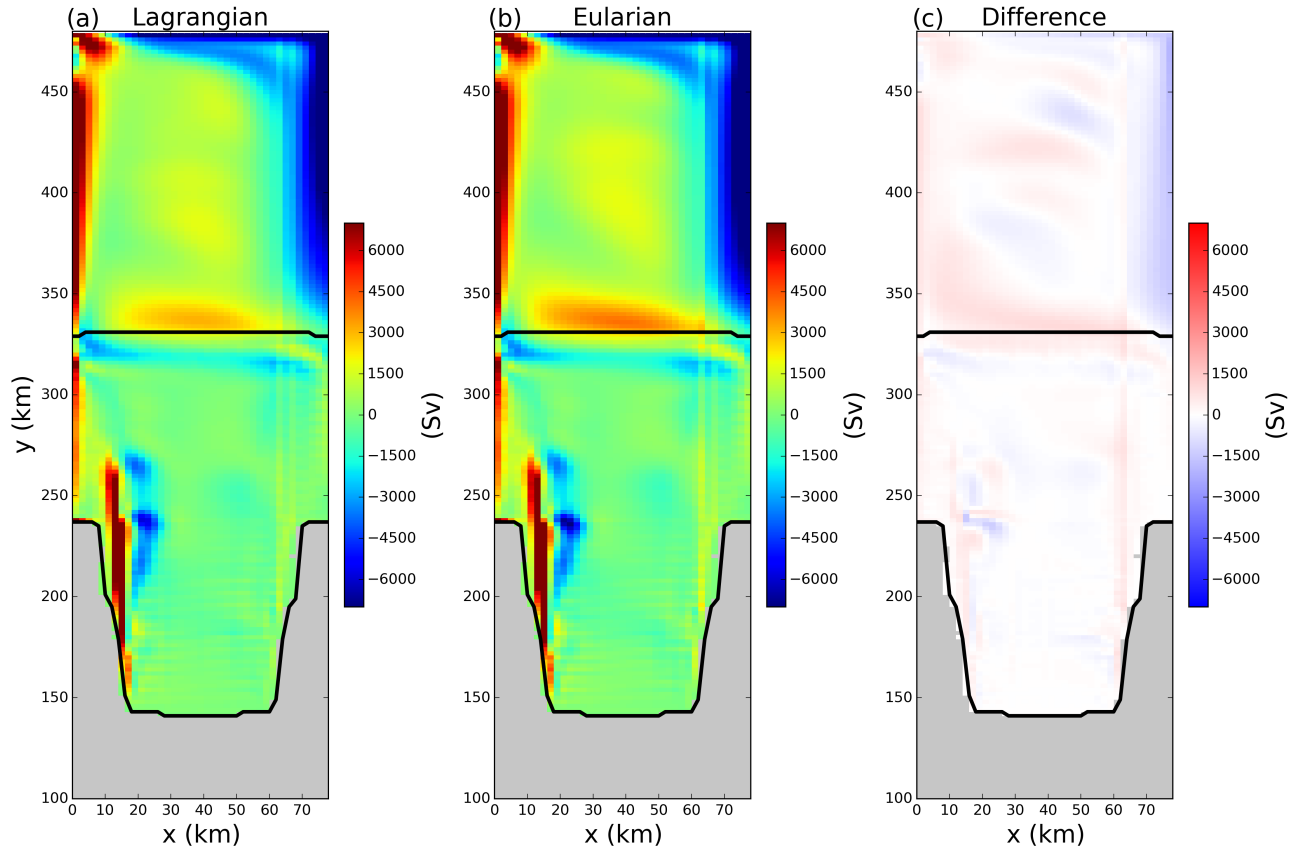


Figure 6. Time-averaged barotropic stream function in the (a) Lagrangian and (b) Eulerian simulations in the static ice-shelf configuration. Panel (c) shows the difference between panels (a) and (b). The time averages are taken over 5 years of model time, beginning at the end of the 5 year spin up period.

Parameter	Symbol	Value	Unit
Domain Length	L_x	80	km
Domain Width	L_y	480	km
Horizontal Resolution	Δx	2	km
Number of vertical layers	N_l	72	non-dim
Horizontal Viscosity	ν_H	6.0	$\frac{m^2}{s}$
Diapycnal Viscosity	ν_V	10^{-3}	$\frac{m^2}{s}$
Horizontal Diffusivity	ϵ_H	1.0	$\frac{s}{m^2}$
Diapycnal Diffusivity	ϵ_V	5×10^{-5}	$\frac{s}{m^2}$
Initial Surface Temperature	T_t	-1.9	$^{\circ}C$
Initial Bottom Temperature	T_b	1.0	$^{\circ}C$
Initial Surface Salinity	S_t	33.8	psu
Initial Bottom Salinity	S_b	34.7	psu
Maximum Ocean depth	H_{ocean}	720	m
Relaxation Time of Sponge Layer	T_{sponge}	0.1	days
Time Step for Static Shelf Experiment	dt_{Static}	1000	s
Time Step for Iceberg Calving Experiment	$dt_{Calving}$	10	s

6. Supplementary Figures

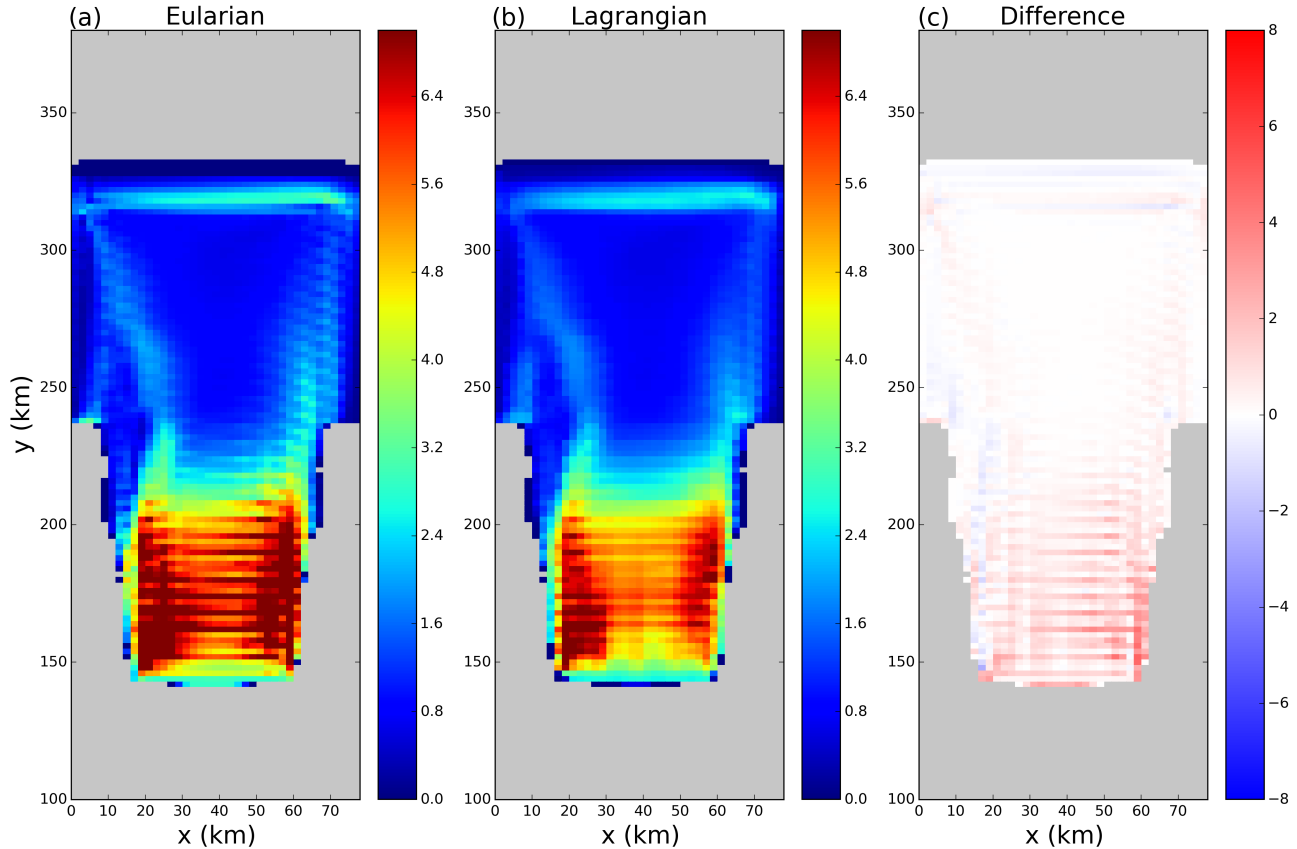


Figure S1. Time-averaged melt rates in the (a) Lagrangian and (b) Eulerian simulations in the static ice-shelf configuration. Panel (c) shows the difference between panels (a) and (b). The time averages are taken over 5 years of model time, beginning at the end of the 5 year spin up period.

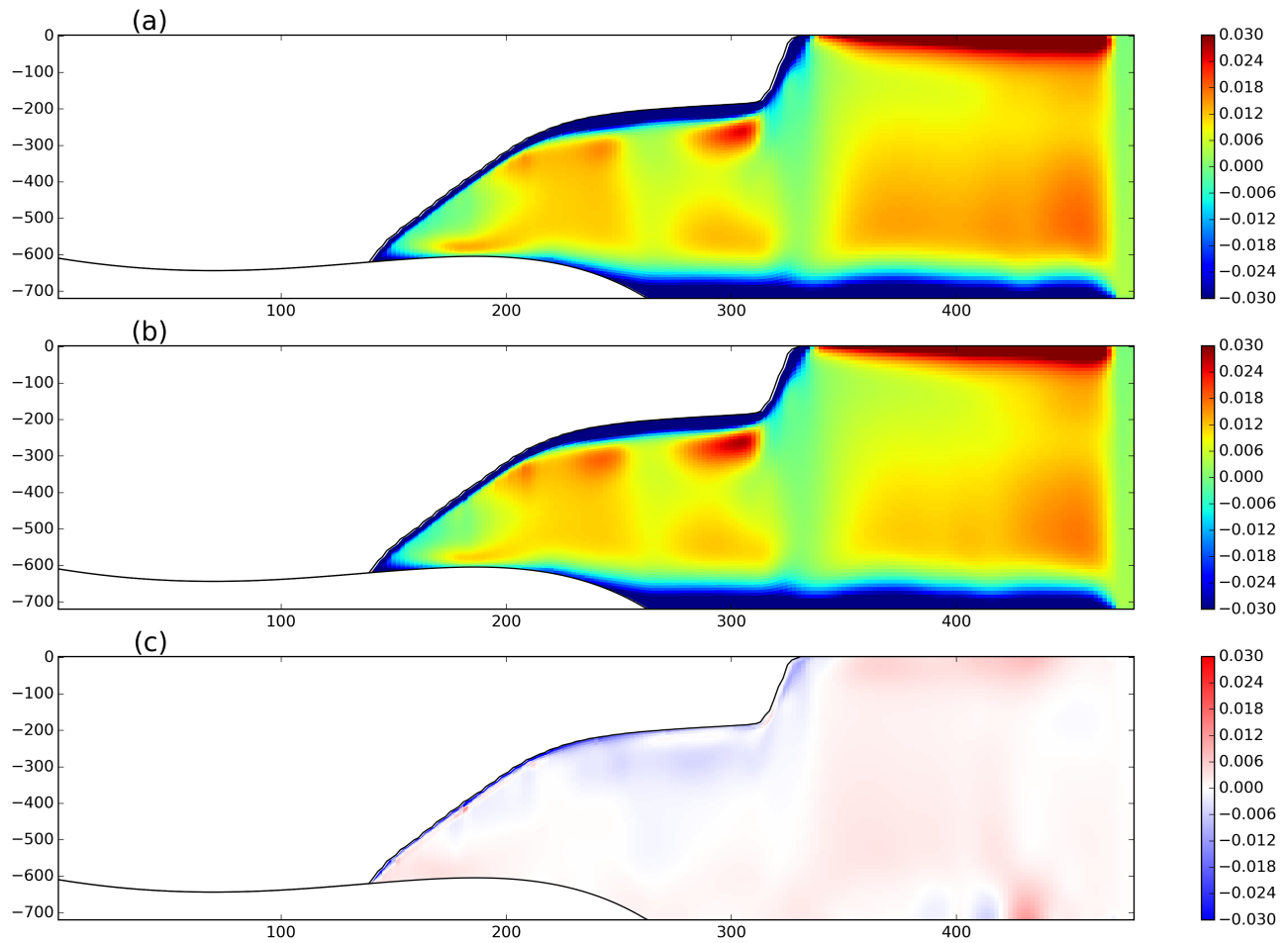


Figure S2. Time-averaged vertical sections of salinity in the (a) Lagrangian and (b) Eulerian simulations in the static ice-shelf configuration at $x=54$ km. Panel (c) shows the difference between panels (a) and (b). The time averages are taken over 5 years of model time, beginning at the end of the 5 year spin up period.